





# Indirect Interspecies Regulation: Transcriptional and Physiological Responses of a Cyanobacterium to Heterotrophic Partnership

 Hans C. Bernstein,<sup>a,e</sup> Ryan S. McClure,<sup>a</sup> Vera Thiel,<sup>c</sup> Natalie C. Sadler,<sup>a</sup> Young-Mo Kim,<sup>a</sup> William B. Chrisler,<sup>a,b</sup> Eric A. Hill,<sup>a</sup>  Donald A. Bryant,<sup>c,d</sup> Margaret F. Romine,<sup>a</sup> Janet K. Jansson,<sup>a</sup> Jim K. Fredrickson,<sup>a</sup> Alexander S. Beliaev<sup>a</sup>

Biological Sciences Division, Pacific Northwest National Laboratory, Richland, Washington, USA<sup>a</sup>; Environmental Molecular Sciences Laboratory, Pacific Northwest National Laboratory, Richland, Washington, USA<sup>b</sup>; Department of Biochemistry and Molecular Biology, The Pennsylvania State University, University Park, Pennsylvania, USA<sup>c</sup>; Department of Chemistry and Biochemistry, Montana State University, Bozeman, Montana, USA<sup>d</sup>; The Gene and Linda Voiland School of Chemical Engineering and Bioengineering, Washington State University, Pullman, Washington, USA<sup>e</sup>

**ABSTRACT** The mechanisms by which microbes interact in communities remain poorly understood. Here, we interrogated specific interactions between photoautotrophic and heterotrophic members of a model consortium to infer mechanisms that mediate metabolic coupling and acclimation to partnership. This binary consortium was composed of a cyanobacterium, *Thermosynechococcus elongatus* BP-1, which supported growth of an obligate aerobic heterotroph, *Meiothermus ruber* strain A, by providing organic carbon, O<sub>2</sub>, and reduced nitrogen. Species-resolved transcriptomic analyses were used in combination with growth and photosynthesis kinetics to infer interactions and the environmental context under which they occur. We found that the efficiency of biomass production and resistance to stress induced by high levels of dissolved O<sub>2</sub> increased, beyond axenic performance, as a result of heterotrophic partnership. Coordinated transcriptional responses transcending both species were observed and used to infer specific interactions resulting from the synthesis and exchange of resources. The cyanobacterium responded to heterotrophic partnership by altering expression of core genes involved with photosynthesis, carbon uptake/fixation, vitamin synthesis, and scavenging of reactive oxygen species (ROS).

**IMPORTANCE** This study elucidates how a cyanobacterial primary producer acclimates to heterotrophic partnership by modulating the expression levels of key metabolic genes. Heterotrophic bacteria can indirectly regulate the physiology of the photoautotrophic primary producers, resulting in physiological changes identified here, such as increased intracellular ROS. Some of the interactions inferred from this model system represent putative principles of metabolic coupling in phototrophic-heterotrophic partnerships.

**KEYWORDS** consortia, cyanobacteria, heterotroph, microbial interactions, transcriptome

Interspecies microbial interactions are controlled by the genome-encoded functions belonging to individual organisms and from their responses to environmental cues. Community-level responses are a function of all species, including those in low abundance, and comprehensive analyses require species-level resolution (1). Most microbial communities in nature are structurally and functionally complex, and it is technically challenging to make species-specific observations of behavior. Hence, model microbial consortia, maintained under controlled environments, are attractive for interrogating


**Received** 18 November 2016 **Accepted** 30 January 2017 **Published** 7 March 2017

**Citation** Bernstein HC, McClure RS, Thiel V, Sadler NC, Kim Y-M, Chrisler WB, Hill EA, Bryant DA, Romine MF, Jansson JK, Fredrickson JK, Beliaev AS. 2017. Indirect interspecies regulation: transcriptional and physiological responses of a cyanobacterium to heterotrophic partnership. *mSystems* 2: e00181-16. <https://doi.org/10.1128/mSystems.00181-16>.

**Editor** Mark J. Mandel, Northwestern University Feinberg School of Medicine

**Copyright** © 2017 Bernstein et al. This is an open-access article distributed under the terms of the [Creative Commons Attribution 4.0 International license](https://creativecommons.org/licenses/by/4.0/).

Address correspondence to Hans C. Bernstein, [hans.bernstein@pnnl.gov](mailto:hans.bernstein@pnnl.gov).

 Cyanobacteria acclimate to heterotrophic partnership showing evidence of indirect interspecies regulation

the principles by which multispecies interactions mediate the exchange of nutrients, vitamins/cofactors, and energy under different growth conditions and environmental constraints (2–6).

Phototroph-heterotroph partnerships are essentially ubiquitous in photic environments and mediate key biogeochemical and ecological processes on a global scale (7). In this study, we employed a bottom-up approach to infer and test specific interactions occurring within a constructed binary consortium containing a unicellular cyanobacterium, *Thermosynechococcus elongatus* BP-1, and an obligate aerobic heterotroph, *Meiothermus ruber* strain A (here *T. elongatus* and *M. ruber*, respectively). *T. elongatus* is a thermophilic, unicellular cyanobacterium previously investigated in numerous ecophysiological and biotechnological studies (8–13). Its genome is well characterized (14) and was first isolated from a hot spring cyanobacterial mat environment near Beppu, Japan (15). *M. ruber* strain A is an aerobic, heterotrophic thermophile isolated from an enrichment culture of *Synechococcus* sp. strain JA-3-3-Ab, which was sampled from a cyanobacterial mat inhabiting the outflow of Octopus Spring in Yellowstone National Park (WY, USA) (16, 17), and shares 98.6% nucleotide identity to the 16S rRNA gene of a closely related strain, *Meiothermus ruber* DSM 1279 (18). At the genome level, both *M. ruber* strains display substantial functional relatedness with regard to carbohydrate and energy metabolism, including genes for glycolysis, tricarboxylic acid cycle, oxidative pentose phosphate, Entner-Doudoroff, and aerobic respiratory electron transfer pathways (16). Similarly to *M. ruber* DSM 1279, strain A lacks an assimilatory nitrate reduction pathway; hence, it depends upon reduced N sources produced by *T. elongatus* when cocultured in minimal medium containing only nitrate. This consortium was constructed specifically to identify interactions underlying acclimation responses to heterotrophic partnership. Simplified consortia, such as the system presented here, are useful tools for studying microbial interactions at the species level. It is much more difficult to interrogate species-resolved responses to partnership in natural systems, in which membership cannot be controlled. Typically, such studies have invoked only bulk measurements of physiological or biochemical activities derived from the entire community or have examined subsets, focusing on only the dominant members (19).

In this study, analyses were performed on both member species by interrogating transcriptional and physiological data associated with a commensal “producer-consumer” interaction (20). These data were collected across tightly controlled steady states maintained via discrete incident irradiance ( $I_i$ ) and dissolved  $O_2$  tension ( $pO_2$ ) treatments. The strains were chosen because of an obligate dependency of *M. ruber* on cyanobacterium-derived carbon and nitrogen, when the consortium was grown in autotrophic minimal medium containing nitrate. These are representative thermophiles derived from hot spring cyanobacterial mats that are hallmark habitats for high solar  $I_i$  and  $pO_2$  that significantly influence microbial interactions and the ecosystem properties (21–25). We designed controlled cultivation experiments that compared axenic growth of *T. elongatus* to growth in the consortium and concluded that *M. ruber* acted as a commensal partner supported by direct metabolite exchange. We then hypothesized that *T. elongatus* sensed and acclimated to its partner and that this behavior represented indirect interspecies regulation where each species coordinated some transcriptional events in response to the other. We conclude that some of these behaviors that relate to the most foundational functions of life, such as carbon and energy acquisition, may represent generalizable principles for phototroph-heterotroph interactions that can occur in habitats subjected to a dynamic range of light and oxygen tensions.

## RESULTS

**Photoautotrophically supported binary culture.** *T. elongatus* supported heterotrophic growth of *M. ruber* under photoautotrophic growth conditions (i.e.,  $CO_2/HCO_3^-$  as the sole carbon sources) in the defined medium containing nitrate with no vitamin amendments (see Fig. S1 in the supplemental material). Stable compositional and metabolic steady states were maintained under turbidostat control. The relative abundances of *T. elongatus* and *M. ruber* remained stable across the treatments and

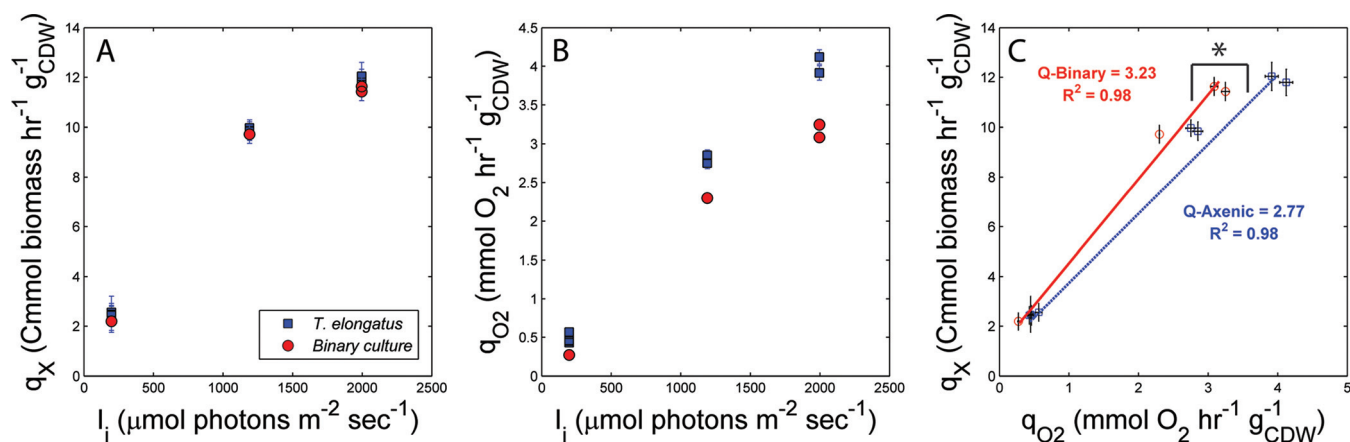


**FIG 1** Growth and photosynthesis kinetics of the *T. elongatus* axenic (blue) and binary (red) cultures held under variable irradiance-controlled turbidostat steady states. (A) Specific growth rates on a Cmol basis. (B) Specific rate of net  $\text{O}_2$  production (net photosynthesis). (C) Growth rate plotted against net photosynthesis. The slope of these curves represents the photosynthetic quotients or yields of carbon uptake into biomass per net photosynthetic output. Each data point represents the average of measurements taken every minute over a minimum of three reactor residence times held under each respective steady state. Error bars represent  $\pm 1$  standard deviation. \*, significant differences with  $>99\%$  certainty as determined by *t* test of unequal sample sizes, assuming equal variance; CDW, cell dry weight.

maintained average values of  $90.2\% \pm 2.0\%$  and  $9.1\% \pm 1.5\%$  cell counts, respectively. Because *M. ruber* lacks the ability to assimilate nitrate (16) (Fig. S2), its capacity to maintain a stable population indicates that a consistent flux of both organic carbon and organic/assimilated nitrogen emanates from the cyanobacterium. Relative extracellular metabolite measurements (i.e., peak area of quantifiable metabolites) confirmed that organic carbon and nitrogen were available for heterotrophic growth and present in the form of citric acid and several amino acids, respectively, although compounds in lower abundance were not accounted for (Fig. S3).

Turbidostat steady states, controlled by incident irradiance ( $I_i$ ), yield the respective maximum specific growth rates ( $\mu$ ) for each condition. Axenic *T. elongatus* and the binary culture  $\mu$  values increased with  $I_i$  values that were between  $350$  and  $2,000 \mu\text{mol photons m}^{-2} \text{s}^{-1}$ . Cell growth did not saturate or become inhibited within the bounds of experimentally imposed  $I_i$  treatments. The  $\mu$  values measured for the binary consortium were nearly identical to those for the *T. elongatus* axenic control under each  $I_i$  treatment. The cultures (binary and axenic) approached 2.4-h doubling times at the highest  $I_i$  treatments ( $2,000 \mu\text{mol photons m}^{-2} \text{s}^{-1}$ ). As expected, analysis of the specific growth rate, on a carbon-mole basis ( $\text{Cmmol biomass h}^{-1} \text{g}_{\text{cell dry weight}}^{-1}$ ), indicated that heterotrophic partnership had a negligible effect on the net conversion of inorganic carbon to biomass compared to the *T. elongatus* axenic control (Fig. 1A). The specific rates of  $\text{O}_2$  production measured in the binary consortium were lower than those in the *T. elongatus* axenic control (Fig. 1B). Hence, the photosynthetic quotients, approximated here as the Cmol fixed into biomass by moles  $\text{O}_2$  produced, were greater in the binary culture than in the *T. elongatus* axenic control (Fig. 1C). The binary culture captured more of its reductant in biomass than did axenic *T. elongatus* as a result of concurrent heterotrophic growth, inferred to be supported by cyanobacterium-derived reduced carbon and nitrogen sources.

**Interaction leads to reduced oxygen sensitivity.** The binary consortium exhibited a decreased sensitivity to  $\text{O}_2$  stress compared to the *T. elongatus* axenic control (Fig. 2). A linear decrease in  $\mu$  was observed, for both the axenic and binary cultures, as the partial pressure of  $\text{O}_2$  ( $p\text{O}_2$ ; corresponding to inlet gas composition) was raised from 0 through 0.59. This decrease was ameliorated in the binary culture. The maximum  $p\text{O}_2$  treatment provided a dissolved  $\text{O}_2$  concentration of  $366 \mu\text{M}$  or 281% of air saturation (at  $52^\circ\text{C}$ ). Oxygen sensitivities were measured as the absolute slope(s)  $0.127 \pm 0.004$  and  $0.086 \pm 0.005 \text{ h atm-O}_2^{-1}$  ( $\pm$  standard error) for the *T. elongatus* axenic control and binary consortium, respectively.

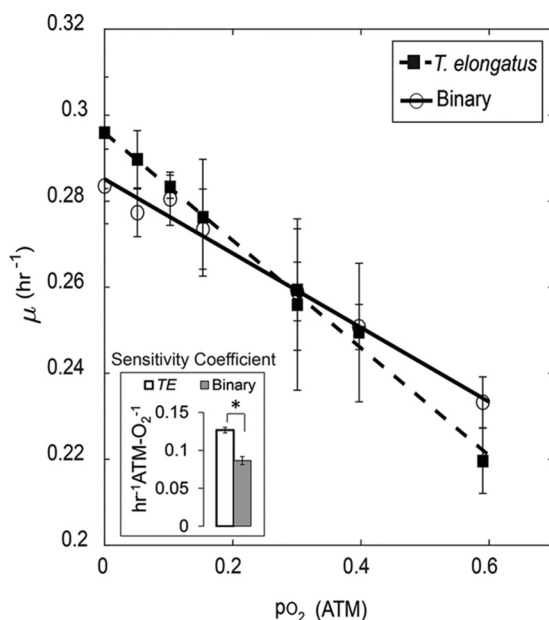


**FIG 2** Oxygen inhibition profiles of steady-state specific growth rates controlled under increasing oxygen tensions ( $pO_2$  of in-gas). The absolute value of the slopes represents the sensitivity coefficients which are inversely proportional to the growth resistance to  $O_2$  stress for each culture. The sensitivity coefficients were determined to be  $0.127 \pm 0.004$  and  $0.086 \pm 0.005$  ( $\pm$  standard error) for the *T. elongatus* axenic (TE) and binary (Binary) cultures, respectively. Each data point represents the average of measurements taken every minute over a minimum of three reactor residence times held under each respective steady state. Error bars represent  $\pm 1$  standard deviation. \*, significant differences with  $>99\%$  certainty as determined by t test of unequal sample sizes, assuming equal variance.

**Cyanobacterial responses to heterotrophic partnership.** *T. elongatus* showed a different transcriptional response in the presence of *M. ruber* than the axenic control. Light- and  $O_2$ -responsive genes were defined as those showing  $\geq 2$ -fold change between the lower and maximum experimental bounds with respect to  $I_i$  and  $pO_2$ . Of the 2,476 protein-encoding genes in *T. elongatus*, 354 and 339 were determined to be light responsive under axenic and binary steady-state conditions ( $pO_2 = 0 \text{ atm-}O_2$ ), respectively. Similarly, 105 and 60 genes were determined to be  $O_2$  responsive under axenic and binary steady-state conditions ( $I_i = 1,995 \mu\text{mol photons m}^{-2} \text{ s}^{-1}$ ), respectively. Different gene function categories were significantly enriched ( $P < 0.05$ ) from groups determined to be either light or oxygen regulated (Fig. 3).

Genes whose transcripts were shown to be responsive by increasing with irradiance included those associated with photosystem II (PS II) (*psbV*, *psbX*, and *psbV2*; *tll1285*, *tsr2013*, and *tll1284*) and  $\beta$ -carboxysome (*ccmK1* and *ccmL*; *tll0946* and *tll0945*) functions. In addition to their response to  $I_i$ , a greater number of PS II genes showed elevated transcript abundance during heterotrophic partnership (Fig. 3A). *T. elongatus* genes encoding significantly enriched functions related to pyruvate metabolism (*pdhB* and *pdhA*; *tll0204* and *tll1169*) and metabolism of the amino acids cysteine and methionine (*cysE* and *metE*; *tll0851* and *tll1190*; *coaX* and *panC-cmk*; *tll1149* and *tll2450*) were light responsive with  $I_i$ , but a smaller number of these genes exhibited such changes in expression as a result of *M. ruber* partnership compared to axenic growth (Fig. 3B).

The majority of functions involving  $O_2$ -responsive genes showed higher enrichment ratios under binary than under axenic *T. elongatus* growth. These include PS I-stabilizing products, peroxide detoxification, and assembly of iron-sulfur clusters. The specific genes in these categories which showed increased expression with  $pO_2$  include photosystem-stabilizing genes *hliC* and *hliA* (*tsr0446* and *tsl2208*), iron sulfur genes *sufD* and *iscU* (*tll1905* and *tll1093*), and peroxide detoxification genes *grxD* (*tll0874*) and *tll1454* (Fig. 3C). Among genes showing decreased expression with increasing  $O_2$ , both type II restriction modification system gene *tll1944* and ornithine biosynthesis gene *argJ* (*tll1911*) were enriched only under axenic conditions.

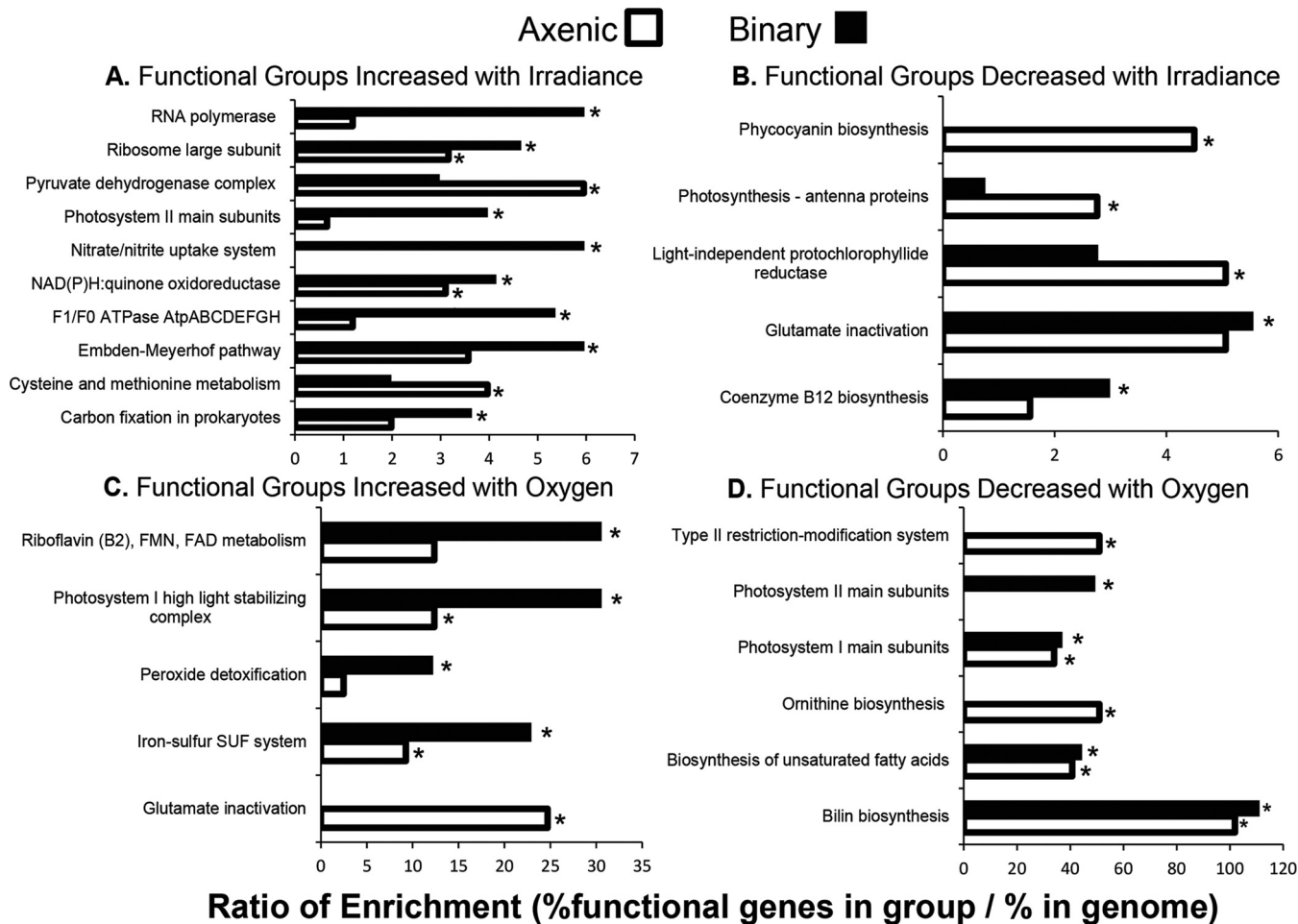


**FIG 3** Enriched gene functions responding to irradiance and  $pO_2$ . Ratios on the x axis depict the percentage of genes of a particular function (shown on the y axis) in a given category (e.g., RNA polymerase genes increasing their expression with irradiance under binary conditions, top black bar of the upper left figure) divided by the percentage of genes of the same function in the genome as a whole. For comparison, the ratios of functional enrichment are shown for both axenic (white) and binary (black) cultivation with at least one of the two being significantly enriched with a  $P$  value of  $<0.05$  as determined by Fisher's exact test (indicated by \*). (A) Functional groups that increased with increasing irradiance. (B) Functional groups that decreased with increasing irradiance. (C) Functional groups that increased with increasing  $O_2$  tension ( $pO_2$ ); SUF, sulphur assimilation. (D) Functional groups that decreased with increasing  $O_2$  tension. FMN, flavin mononucleotide; FAD, flavin adenine dinucleotide.

Another acclimation response to partnership was observed as increased relative intracellular abundances of reactive oxygen and nitrogen species (ROS and RNS, respectively) during binary cultivation compared to the *T. elongatus* axenic controls (Fig. 4). The fluorescence of an oxidized ROS-RNS reporter dye [5-(6-chloromethyl-2',7'-dichlorodihydrofluorescein diacetate, acetyl ester (CM-H<sub>2</sub>DCFHAD)] increased under binary cultivation but, unexpectedly, was insensitive to the increasing  $pO_2$  treatments. *T. elongatus* showed differential expression of ROS detoxification transcripts in the presence of *M. ruber* across a broad range of  $I_l$ - and  $pO_2$ -controlled steady states. In many cases, the expression patterns of these *T. elongatus* transcripts showed opposite trends between axenic and binary cultivation across the  $I_l$  and  $pO_2$  treatments (Fig. 5). Generally, an increased relative abundance of these transcripts was observed under binary cultivation compared to the *T. elongatus* axenic control. These results show that *T. elongatus* acclimates to partnership with *M. ruber* by changing the expression of ROS detoxification genes, which is likely driven by a heterotrophically mediated increase in ROS-RNS.

**Coordinated transcriptional patterns as a result of metabolic coupling.** A guiding hypothesis was that since *T. elongatus* supported *M. ruber* via exchange of essential resources (i.e., C, N, and  $O_2$ ), *M. ruber* must coordinate its gene expression to

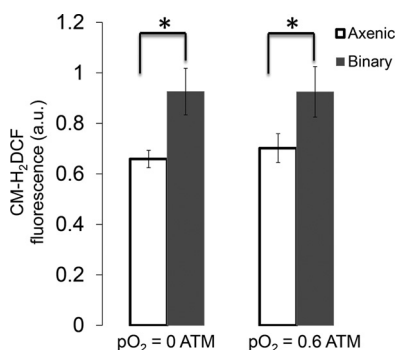


**FIG 4** Intracellular reactive oxygen/nitrogen (ROS-RNS) increased under binary cultivation compared to axenic *T. elongatus* controls. Average intensity ( $n = 3$ ) of the 525-nm fluorescence emitted from cells excited at 488 nm, corresponding to the abundance of oxidized ROS-RNS reporter dye (CM-H<sub>2</sub>DCFHDA) for the *T. elongatus* axenic and binary cultures maintained under low and high oxygen tensions. Error bars represent  $\pm 1$  standard deviation. \*, significant differences with  $>99\%$  certainty as determined by Tukey's test.

accommodate the variable physiology of the cyanobacterium across the gradients of  $I_i$  and  $pO_2$  conditions. Examination of individual transcript profiles was performed by considering clusters around four main patterns specified by the centroid or "eigen-genes" corresponding to the  $I_i$  and  $pO_2$  treatments used to establish steady state (Fig. 6). Clusters A to D were calculated to examine responses to  $I_i$  treatments, and clusters E to H were calculated for examining the transcriptional effects from increasing  $O_2$  tension. All clusters contained both *T. elongatus* and *M. ruber* genes. Cluster A exhibits a tent-shaped eigen-gene with maximum relative mRNA abundances at the midpoint  $I_i$  (1,190  $\mu\text{mol photons m}^{-2} \text{s}^{-1}$ ). The midpoint was chosen as a sampling condition because it is the theoretical saturating irradiance (26). Genes in cluster B responded inversely to those in cluster A. Clusters C and D contain genes that show a relative

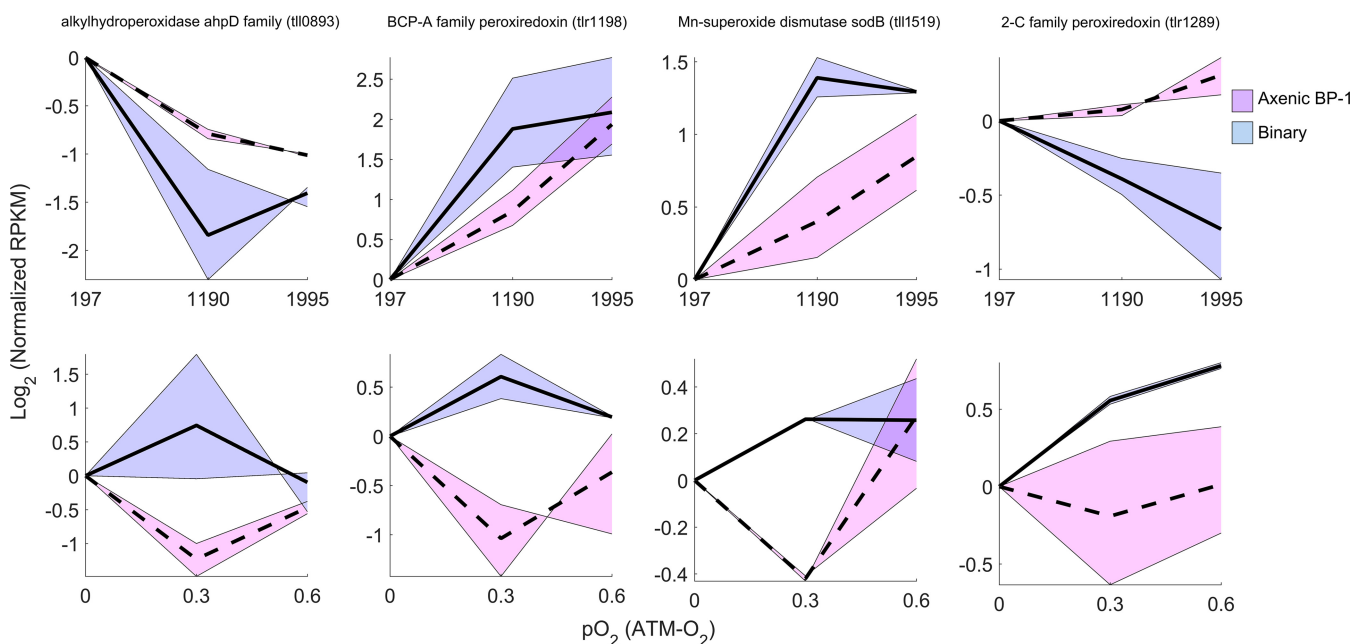


**FIG 5** Relative abundance profiles for *T. elongatus* transcripts of ROS-RNS detoxification genes that showed at least a 1.5-fold change over either the irradiance- or  $pO_2$ -controlled steady states. Solid black lines and shaded blue regions represent the means and ranges of *T. elongatus* genes expressed during binary cultivation. Similarly, dashed black lines and shaded red regions represent the means and ranges of *T. elongatus* genes expressed during axenic cultivation. The transcripts identified include a putative alkyhydroperoxidase *ahpD* family gene (*tlh0893*), a BCP-A family peroxiredoxin (*tlr1198*), an Mn-superoxide dismutase (*sodB*; *tlh1519*), and a 2-Cys family peroxiredoxin (*tlr1289*). "Normalized RPKM" is the average of duplicate RPKM values measured under each steady state divided by the average RPKM corresponding to the lowest incident irradiance (197  $\mu\text{mol photons m}^{-2} \text{s}^{-1}$ ) or  $pO_2$  (0 atm- $O_2$ ).

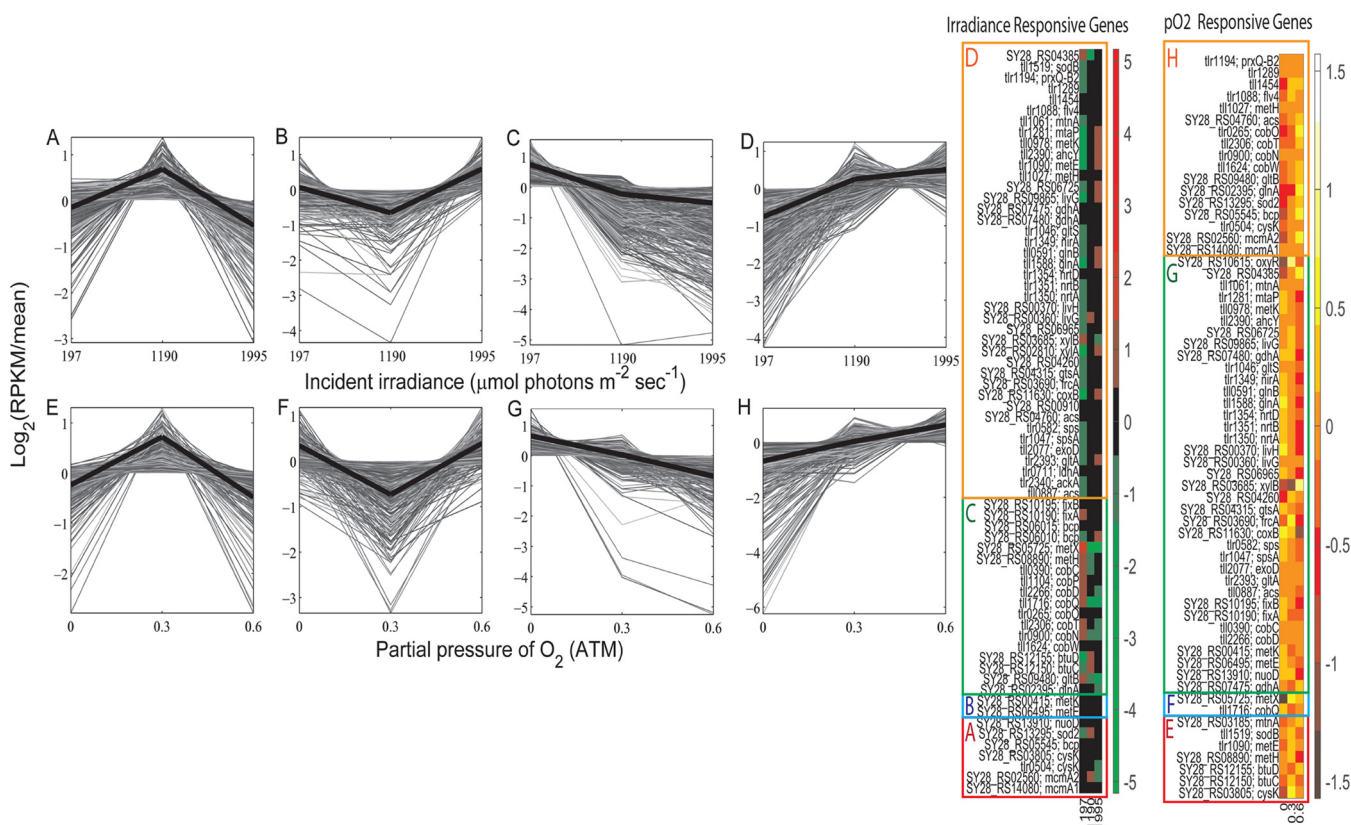


**FIG 6** K-means clusters of *T. elongatus* and *M. ruber* relative mRNA abundance profiles that share correlated expression patterns over irradiance- and pO<sub>2</sub>-controlled steady states. Heavy black lines represent the centroid (i.e., eigen-gene) calculated within each cluster. Cluster A, 201 *T. elongatus* plus 259 *M. ruber* genes; cluster B, 255 *T. elongatus* plus 188 *M. ruber* genes; cluster C, 971 *T. elongatus* plus 444 *M. ruber* genes; cluster D, 914 *T. elongatus* plus 324 *M. ruber* genes; cluster E, 211 *T. elongatus* plus 328 *M. ruber* genes; cluster F, 187 *T. elongatus* plus 309 *M. ruber* genes; cluster G, 913 *T. elongatus* plus 468 *M. ruber* genes; cluster H, 888 *T. elongatus* plus 387 *M. ruber* genes. Heat maps show the expression patterns [log<sub>2</sub>(RPKM/mean)] for specific functional genes from each organism.

decrease or increase with I<sub>i</sub>, respectively. Note that the changes observed for the relative abundance of transcripts with increasing I<sub>i</sub> also correspond to increasing specific growth and photosynthesis rates (Fig. 1). Clusters E to H contain transcripts that trend with increasing pO<sub>2</sub> treatments (0 to 0.59 atm-O<sub>2</sub>) and show profiles that are analogous to clusters A to D. Changes observed for the relative abundance of transcripts with increasing pO<sub>2</sub> correspond to a linear decrease in the specific growth rate (Fig. 2). Statistically enriched gene functions were identified for both *T. elongatus* and *M. ruber* within each cluster (Tables S1 and S2) to infer which processes may have been involved in metabolite exchange and acclimation to partnership.

**Primary productivity and carbon exchange.** *T. elongatus* supported *M. ruber* growth via the production and transfer of reduced carbon. Cyanobacterial processes involved in biosynthesis and transport of organic carbon shared common transcriptional patterns with *M. ruber* genes encoding enzymes used in carbon uptake and metabolism of the same (or similar) gene products. Principal genes involved in organic acid synthesis of *T. elongatus* grouped into clusters that increased with I<sub>i</sub> (cluster D) and/or decreased with pO<sub>2</sub> (cluster G). These included acetyl coenzyme A (CoA) synthetase (*acs*; *tl10887*), acetate kinase (*ackA*; *tlr2340*), lactate dehydrogenase (*ldhA*; *tlr0711*), and citrate synthase (*gltA*; *tlr2393*). Functions involved in synthesis and export of larger biomolecules (i.e., sugars, peptides, and extracellular polymeric substance [EPS]) also grouped into clusters D and G. These included a putative exopolysaccharide synthesis gene (*exoD*; *tl12077*), sucrose synthase (*spsA*; *tlr1047*), and a sucrose degradation enzyme (*sps*; *tlr0582*). In conjunction with *T. elongatus*, *M. ruber* genes involved in the uptake and metabolism of compounds related to export and synthesis of *T.*

Downloaded from <http://mSystems.asm.org/> on December 5, 2017 by guest

*elongatus*-derived organic carbon were also found in clusters D and/or G. Notable examples included genes encoding putative acetyl-CoA synthetase (*acs*; SY28\_RS04760 and SY28\_RS00910), cytochrome *c* oxidase (*coxB*; SY28\_RS11630), monosaccharide uptake systems (*frcA* and *gtsAB*; SY28\_RS03690, SY28\_RS04315, and SY28\_RS04260), xylose isomerase (*xylA*; SY28\_RS02810), xylulokinase (*xylB*; SY28\_RS03685), an ABC-type multisugar uptake system (SY28\_RS06965), and branched-chain amino acid uptake (*livGH*; SY28\_RS00360 and SY28\_RS00370).

**Nitrogen and amino acid exchange.** Since *M. ruber* lacks an assimilatory nitrate reductase, *T. elongatus* was assumed to provide reduced N during binary cultivation. The relative abundances of transcripts encoding the *T. elongatus* nitrate uptake system from *nrtABD* (*tlr1350*, *tlr1351*, and *tlr1354*) increased with  $I_i$ , decreased with  $pO_2$ , and grouped appropriately into clusters D and G. Other *T. elongatus* nitrogen metabolism genes found in these clusters include glutamine synthetase gene *glnA* (*tll1588*), a nitrogen regulatory protein gene (*glnB*; *tll0591*), an assimilatory ferredoxin-nitrate reductase gene (*nirA*; *tlr1349*), and a glutamate symporter gene (*gltS*; *tlr1046*). Several *M. ruber* nitrogen-associated genes also grouped into clusters D and/or G, including a glutamate dehydrogenase gene (*gdhA*; SY28\_RS07480 and SY28\_RS07475) and amino acid uptake system genes (SY28\_RS09865 and SY28\_RS06725). However, some key genes required for N acquisition by *M. ruber* grouped into clusters C and/or H, showed opposite expression patterns with respect to  $I_i$  and  $pO_2$ , and effectively increased with the specific growth and photosynthesis rates. These include *glnA* (SY28\_RS02395) and the large subunit of glutamate synthase (*gltB*; SY28\_RS09480) and suggest the potential for direct exchange of glutamine and glutamate from *T. elongatus* as growth requirements increase with the specific growth and photosynthesis rates.

**Methionine and vitamin B<sub>12</sub> exchange.** Cobalamin (B<sub>12</sub>) auxotrophy in *M. ruber* is indicated by the absence of a complete B<sub>12</sub> synthesis pathway and a B<sub>12</sub>-independent methylcitrate pathway (*prpBCDF*) required for conversion of propionyl-CoA to succinyl-CoA. *M. ruber* contains the vitamin B<sub>12</sub>-dependent methylmalonyl-CoA mutase subunits (*mcmA1* and *-A2*; SY28\_RS14080 and SY28\_RS02560) which grouped into clusters A and H. *T. elongatus* is a B<sub>12</sub> prototroph, as confirmed by the capacity for axenic growth in the absence of vitamin B<sub>12</sub> and by the presence of a complete vitamin B<sub>12</sub> biosynthesis pathway in the genome. The relative abundances of transcripts encoding vitamin B<sub>12</sub> uptake/scavenging gene products in *M. ruber* (*btuCD*; SY28\_RS12150 and SY28\_RS12155) decreased with  $I_i$  in concurrence with decreased *T. elongatus* transcripts (all within cluster C) encoding vitamin B<sub>12</sub> biosynthesis, including those required for the insertion of cobalt (*cobWNT*; *tll1624*, *tlr0900*, and *tll2306*) and for the conversion of cobyrinic acid diamine to the vitamin B<sub>12</sub> coenzyme from *cobOQDPC* (*tlr0265*, *tll1716*, *tll2266*, *tll1104*, and *tll0390*). Both *T. elongatus* and *M. ruber* expressed transcripts encoding the vitamin B<sub>12</sub>-dependent homocysteine methyltransferase (*metH*) but were negatively correlated and grouped across  $I_i$  and  $pO_2$  treatments into opposing clusters D (*tll1027*) and C (SY28\_RS08890), indicating that methionine may be directly exchanged from *T. elongatus* as growth requirements increase with the specific growth rate. Both strains also expressed vitamin B<sub>12</sub>-independent homocysteine methyltransferase (*metE*) transcripts which grouped into clusters D and E compared to clusters B and G for *tlr1090* and SY28\_RS06495, respectively.

The relative abundances of *T. elongatus* transcripts encoding the degradation and salvage of methionine (*ahcY*, *metK*, *mtaP*, and *mtnA*; *tll2390*, *tll0978*, *tlr1281*, and *tll1061*) increased with  $I_i$  but decreased with  $pO_2$  treatments and grouped within clusters D and G, respectively. Uniform grouping of *M. ruber* transcripts encoding methionine degradation and salvage was not observed as they were spread across multiple clusters grouped by the  $I_i$  and  $pO_2$  treatments: *metK* (SY28\_RS00415; clusters B and G) and *mtnA* (SY28\_RS03185; cluster E). In contrast, the relative abundance of *M. ruber* transcripts encoding methionine biosynthesis proteins decreased with  $I_i$ , and they were grouped into cluster C, including *metHX* (SY28\_RS08890 and SY28\_RS05725). Genes involved in cysteine biosynthesis shared common transcriptional patterning between species,

indicating that while *M. ruber* may have salvaged cyanobacterium-derived methionine, it likely synthesized its own cysteine via the vitamin B<sub>12</sub>-independent pathway as growth requirements increased. These include cysteine synthases (*cysK*; *tlr0504* and *SY28\_RS03805*) and serine O-acetyltransferases (*cysE*; *tlr0851* and *SY28\_RS05065*), which cogenerated into clusters D and A, respectively.

**Oxidative stress responses.** The relative abundance of *T. elongatus* transcripts encoding enzymes involved with ROS detoxification generally increased with increasing I<sub>i</sub> and pO<sub>2</sub>, and the transcripts grouped into the appropriate clusters D and/or H. Notable examples include an NAD(P)H-oxygen oxidoreductase (*flv4*; *tlr1088*), 2-Cys family peroxiredoxins (*tll1454* and *tlr1289*), a periplasmic peroxiredoxin (*prxQ-B2*; *tlr1194*), and an Mn-superoxide dismutase (*sodB*; *tll1519*). *M. ruber* contains an H<sub>2</sub>O<sub>2</sub>-responsive transcriptional regulator (*oxyR*; *SY28\_RS10615*), which grouped into clusters D and G and is located adjacent to a putative manganese catalase (*SY28\_RS10610*). However, *M. ruber* peroxidase (*bcp*; *SY28\_RS05545*, *SY28\_RS06010*, and *SY28\_RS06015*) and superoxide dismutase (*sod2*; *SY28\_RS13295*) genes responded differently to I<sub>i</sub> treatments than did *oxyR* and related cyanobacterial profiles and were grouped into clusters A and C. These genes generally increased with pO<sub>2</sub> and grouped with the *T. elongatus* genes into cluster H (increased with pO<sub>2</sub> and decreasing  $\mu$ ). *M. ruber* genes associated with electron transfer processes that are potentiators of ROS (27, 28) grouped into cluster G, which decreased with increasing pO<sub>2</sub> treatments and increased with specific growth and photosynthesis rates. These include subunits for an electron transfer flavoprotein (*fixAB*; *SY28\_RS10190* and *SY28\_RS10195*), NADH-dehydrogenase (*SY28\_RS04385*), and principal components of the NADH-quinone oxidoreductase (*nuo-DFGHIJKN*).

## DISCUSSION

The cyanobacterium *T. elongatus* responded to heterotrophic partnership with *M. ruber* by altering the expression of key functional genes. This primary result is evidence of indirect interspecies regulation. It is important to note that the turbidostat culturing platform provided a constant, optically thin, nutrient-replete environment. Hence, the addition of *M. ruber* to *T. elongatus* cultures did not alter the growth environment by reducing availability of actinic light or nutrients needed to support *T. elongatus*. The net specific rate of O<sub>2</sub> production decreased during binary cultivation compared to the *T. elongatus* axenic controls. These rates are functionally equivalent to net photosynthesis rates and account for the gross rate of oxygenic photosynthesis minus all oxygen-consuming reactions, including photorespiration (RuBisCO oxygenase activity) and heterotrophic respiration (29, 30). The net photosynthesis rates are conservative interpretations for the lower bound of oxygenic photosynthesis and relatable as proxy measurements for the minimum consortium-wide energy acquisition rates, assuming 0.125 quanta absorbed and 2 NADPH produced per mole O<sub>2</sub> formed via PS II-mediated charge separation (31). Hence, the energy efficiency for biomass production is greater in the binary consortium than in the *T. elongatus* axenic control. These increases likely result from heterotrophic capture of reductant that would otherwise be lost from the system as either photosynthate or necromass. The addition of *M. ruber* partnership also resulted in an observed decrease in O<sub>2</sub> sensitivity compared to *T. elongatus* axenic controls (Fig. 2). A decrease in sensitivity is equivalent to an increase in O<sub>2</sub> stress resistance. We note that this effect was observed under identical pO<sub>2</sub> treatments (binary versus axenic), which supported O<sub>2</sub> tensions sufficient to render the bulk effects resulting from heterotrophic O<sub>2</sub> removal as negligible. However, attachment or close cellular proximity of *M. ruber* to *T. elongatus* cells may create localized gradients and microheterogeneities in I<sub>i</sub> and pO<sub>2</sub> experienced by the *T. elongatus* population. Interactions that occur when cells from each species are in close contact could account for the observed differences in O<sub>2</sub> sensitivity and the photosynthetic quotients which were based on measurements taken from the well-mixed (bulk) volume.

The *M. ruber*-induced decrease of O<sub>2</sub> sensitivity (Fig. 2) originally led us to hypothesize that heterotrophic partnership reduced cyanobacterial oxidative stress and that

this effect could be observed by comparing intracellular ROS-RNS between axenic and binary conditions. Interestingly, we found that heterotrophic partnership had the opposite effect and that increased  $pO_2$  had no effect on intracellular ROS-RNS (Fig. 4). However, the binary culture's observed decrease in  $O_2$  sensitivity did correspond to enrichment of genes within the functional category photosystem I high-light-stabilizing complex (Fig. 3). The *T. elongatus* genes in this category include *hliACD* (*tsl2208*, *tsr0446*, and *tsr1916*) and *tsl0063*, annotated as a member of the CAB/ELIP/HLIP protein family, which are known to be stress-induced genes that help cyanobacteria cope with free radicals and excess excitation energy (32, 33). The increases in ROS-RNS observed as a direct result of heterotrophic partnership corresponded with increased relative transcript abundances of *T. elongatus* genes required for mitigating ROS, showing that the cyanobacterium acclimates to heterotrophic partnership by increasing protection from oxidative stress (Fig. 4 and 5). This is contrary to previous observations made in consortia constructed from oligotrophic cyanobacteria and heterotrophs, in which *Prochlorococcus* species have been reported to benefit and/or depend upon heterotrophic bacteria, such as *Alteromonas*-like species, to reduce oxidative stress (34, 35). In contrast, evidence of cyanobacterium-mediated ROS mitigation was reported within the binary consortium of *Synechococcus* sp. strain PCC 7002 coupled with *Shewanella putrefaciens* W3-18-1, cultured under very different conditions than those employed in the current study (2). Both *T. elongatus* and *Synechococcus* sp. PCC 7002 were isolated from eutrophic environments (mat and marine sediment, respectively), which can presumably support higher levels of heterotrophic growth than oligotrophic marine environments. Cyanobacteria are equipped to detoxify intracellular ROS-RNS and mitigate oxidative stress, because ROS production is an inherent by-product of oxygenic photosynthesis and photosynthetic electron transfer (36, 37), while heterotrophic bacteria are recognized for production of extracellular ROS (27). The principle that is inferred from these collective results is that some cyanobacteria, such as *Synechococcus* species adapted to eutrophic environments exposed to high irradiance, specialize in ROS-RNS mitigation (38, 39).

The metabolic dependency of *M. ruber* upon *T. elongatus* for reduced carbon, nitrogen, and certain vitamins (i.e.,  $B_{12}$ , biotin, and niacin) was corroborated through the coexpression of genes encoding enzymes that metabolize and transport shared metabolites. These inferences are made through the basic assumption that the coexpressed genes, i.e., correlated mRNA abundances between the two species, correspond to protein frequency and activity. Clustering the relative mRNA abundance profiles of the two organisms together provided the means to infer which specific metabolic exchanges are coordinated and how these interactions respond to  $I_i$  and  $pO_2$ . Specifically, the results suggest that multiple carbon compounds derived from the cyanobacterium could be exchanged and taken up by *M. ruber*. While evidence for the exchange of organic acids (e.g., acetate) was observed, polysaccharides, peptides, and EPS may have also supplied the carbon and reductant required to support stable *M. ruber* populations. Ample evidence also supports the likelihood that amino acids can serve as a source of reduced N (and possibly carbon) required by *M. ruber*. For example, the expression of genes involved in the synthesis, transport, and salvage of specific amino acids showed coordinated patterns shared by each species. Specifically, *T. elongatus* transcripts of methionine and glutamate biosynthesis genes clustered into groups that increased with  $\mu$  (clusters D and G) while *M. ruber* homologs showed opposite patterns (clusters C and H), suggesting the specific exchange of these amino acids. The relative abundance profiles for *M. ruber* genes encoding vitamin  $B_{12}$ -dependent methionine synthesis showed expression patterns in common with vitamin  $B_{12}$  salvage and *T. elongatus* vitamin  $B_{12}$  synthesis genes, indicating that one exchanged resource (e.g., vitamin  $B_{12}$ ) may affect requirement of another exchangeable resource (e.g., methionine) that has a closely linked pathway.

The collection of experimental results presented here clearly shows that the cyanobacterium responded and acclimated to heterotrophic partnership. In this experimental system, *T. elongatus* is either indirectly regulated by environmental changes

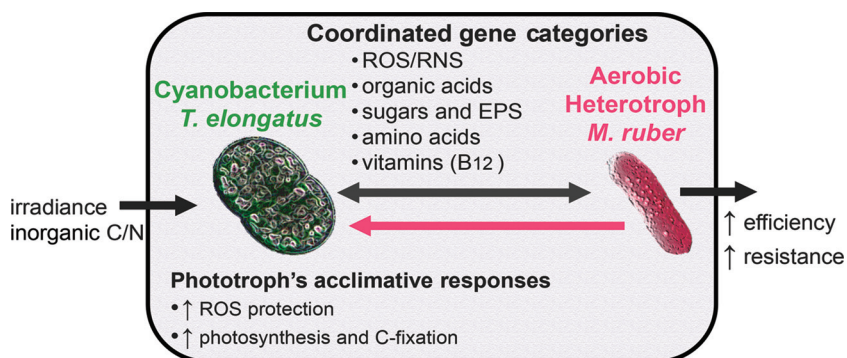


**FIG 7** Schematic outline of responses to heterotrophic partnership observed and inferred as indirect interspecies regulation events and metabolic coupling.

instigated by *M. ruber* or directly regulated via molecular signals. The integrated kinetics- and global transcriptomics-based inferences were not targeted enough to capture a mechanism for direct interspecies regulation. Although direct interspecies regulation cannot be ruled out, our conclusion is that this heterotrophic partnership establishes an indirect interspecies regulation of gene expression resulting in measurable changes of growth and photosynthesis kinetics of the binary culture compared to the cyanobacterial axenic control. The outcomes described here can be generalized to understand microbial cyanobacterium-heterotroph interactions better (Fig. 7). For instance, the cyanobacterium was inferred to sense the presence of its commensal heterotrophic partner and respond by altering its gene expression. Interspecies modulation of gene expression, via indirect regulation, is supported by results reported in previous studies that investigated very different cyanobacterium-heterotroph platforms (2, 4), and a number of notable commonalities emerge. A previous study, investigating a consortium composed of cyanobacterium *Synechococcus* sp. PCC 7002 coupled with *Shewanella putrefaciens* W3-18-1 (2), reported a >2-fold change in mRNA abundances of cyanobacterial genes (compared to axenic) that encode enzymes belonging to the same functional groups that were statistically enriched from *T. elongatus* in the current study (Fig. 3). These include some of the most notable examples, such as carbon concentration, carboxysome synthesis, PS II, oxidative phosphorylation, methionine metabolism, and Fe-S cluster biogenesis. Similarly to the results from this study, *Synechococcus* sp. PCC 7002 was also reported to show >2-fold changes in B<sub>12</sub> salvage processes when partnered with *S. putrefaciens* W3-18-1, although the current study investigated a cyanobacterial B<sub>12</sub> prototroph. Another study, which investigated the transcriptional responses of *Synechococcus* sp. WH8102 cocultured with *Vibrio parahaemolyticus*, also reported changes in expression of genes sharing the functions reported here. These include amino acid biosynthesis, cofactor biosynthesis, PS II, NAD(P)H-dehydrogenase, and ATPase. The functional similarities of cyanobacterial genes being influenced and potentially indirectly regulated by the activity of a heterotrophic partner are remarkable considering the difference in species, their origins, and the treatments and culturing platforms compared. Interspecies modulation of gene expression likely serves as a fundamental principle enabling microbial communities to coordinate their metabolism and coacclimate to each other and environmental cues.

## MATERIALS AND METHODS

**Bacterial strains and culturing media.** Both *Thermosynechococcus elongatus* strain BP-1 and *Meiothermus ruber* strain A were grown axenically and as a binary consortium in a modified BG-11 (mBG-11) medium (BP-1 medium) containing 17.6 mM NaNO<sub>3</sub>, 0.304 mM MgSO<sub>4</sub>·7H<sub>2</sub>O, 0.175 mM KH<sub>2</sub>PO<sub>4</sub>, 0.245 mM CaCl<sub>2</sub>·2H<sub>2</sub>O, 0.0028 mM Na<sub>2</sub>EDTA, and 0.0144 mM FeCl<sub>3</sub>. The mBG-11 was supplemented with 1 ml liter<sup>-1</sup> trace mix: 46.2544 mM H<sub>3</sub>BO<sub>3</sub>, 9.1458 mM MnCl<sub>2</sub>·4H<sub>2</sub>O, 0.772 mM ZnSO<sub>4</sub>·7H<sub>2</sub>O, 1.611 mM Na<sub>2</sub>MoO<sub>4</sub>·2H<sub>2</sub>O, 0.316 mM CuSO<sub>4</sub>·5H<sub>2</sub>O, and 0.170 mM Co(NO<sub>3</sub>)<sub>2</sub>·6H<sub>2</sub>O. During binary culture, both species were supported by the autotrophic growth of *T. elongatus* (i.e., no organic substrate was added for the growth of *M. ruber*). Axenic starter cultures of *M. ruber* were cultured in mBG-11 supplemented with 1% yeast extract. Starter cultures were generated in 150-ml sealed serum bottles

charged with 50 ml mBG-11 plus 15 mM NaHCO<sub>3</sub> (adjusted to pH 7.5) under 10% CO<sub>2</sub> in N<sub>2</sub> headspace. Photobioreactors were inoculated to an optical density at 730 nm (OD<sub>730</sub>) of 0.01 with exponentially growing starter culture(s).

**Turbidostat photobioreactor operation.** This study modified a previously reported continuous stirred tank reactor operated with feedback control as a turbidostat (40–43). Briefly, a “white-light” photobioreactor (7.5-liter vessel) was constructed with evenly spaced sets of fluorescent lights (Sylvania; model FP14/835/ECO, Pentron 3500 K, 14 W) at each quadrant of the cylindrical bioreactor vessel (both 8- and 12-bulb configurations). A custom dimmer was controlled with a 4- to 20-mA signal commanded from a New Brunswick Scientific BioFlo 310 bioreactor controller. The reactor and light bank apparatus were isolated from external ambient light. The working volume of the reactor (5.5 liters) was held at a constant temperature of 52°C and pH 7.5. A Clark-type oxygen sensor coupled with two independent off-gas sensors (Blue Sense; Cell and Ferm models) was used to measure dO<sub>2</sub> and off-gas O<sub>2</sub> and CO<sub>2</sub>, respectively. Incident scalar irradiance and the transmitted irradiance used to control turbidostat operation were maintained using custom photovoltaic cells coupled with a digital pA/mV multimeter (Keithley 2700 Integra Series; Tektronix, Beaverton, OR). The dilution rate of the culture was determined gravimetrically from the effluent medium. Steady states were defined by stable (<10% variation from the mean) measurements of dilution rate, OD<sub>730</sub>, and dissolved O<sub>2</sub> for a minimum of 3 residence times. These measurements, as well as off-gas CO<sub>2</sub>, pH, temperature, and acid/base addition, were data logged at 1-min intervals; hence, the replication of values used to calculate the specific rates (presented in Fig. 1 and 2) is means and standard deviations from a minimum of 604 measurements (for the fastest residence time of 3.36 h; dilution). Additional details for bioreactor-enabled measurements are available in Text S1 in the supplemental material.

**Flow cytometry.** The flow cytometry data were obtained using a BD Influx fluorescence-activated cell sorter (FACS; BD Biosciences, San Jose, CA). Using the 488-nm excitation from a Sapphire LP laser (Coherent Inc., Santa Clara, CA) at 100 mW, samples were analyzed using a 70- $\mu$ m nozzle. Optimization and calibration of the FACS were performed before each analysis using 3- $\mu$ m Ultra Rainbow fluorescent particles (Spherotech, Lake Forest, IL). The ratio of the two distinct populations of cells within a mixed microbial community was identified from 50,000 recorded cells using size and complexity gates with FCS Express (Los Angeles, CA) flow cytometry software. Cell counts are presented as the percentage of total counting events.

**RNA isolation and sequencing.** Cells for total RNA isolation were harvested from steady-state growth conditions by previously reported methods (2, 43). Transcriptomic samples were sampled in a minimum of two biological duplicates sampled from steady states in a minimum of 1 residence time (1/dilution rate) apart from each other. Briefly, cells were collected via centrifugation at 7,000 rpm for 5 min at 4°C, frozen in liquid nitrogen, and stored at –80°C. All RNA analyses were repeated in biological duplicates. To analyze the response of *T. elongatus* alone to the addition of a heterotrophic partner, RNA was extracted with TRIzol and sequenced using SOLiD (sequencing by oligonucleotide ligation and detection) technology with no depletion of rRNA (see the supplemental material for details). However, as binary culture samples contained <10% *M. ruber* by cell count, the extraction and sequencing methodology was modified when collecting data used to specifically examine the correlation of transcriptional responses between *T. elongatus* and *M. ruber*. For this, RNA was extracted using the SV total RNA isolation system (Promega, Madison, WI) followed by genomic DNA removal and purification using the Turbo DNA-free kit (Life Technologies, Carlsbad, CA). An Agilent 2100 Bioanalyzer was used to assess the integrity of the RNA samples. Only RNA samples having an RNA integrity number between 8 and 10 were used. cDNA libraries were constructed using the Ovation Universal transcriptome sequencing (RNA-seq) system (NuGEN, San Carlos, CA). This kit was used to incorporate specific InDA-C probes used to deplete rRNA from the binary culture experiments. Probes were designed to deplete both 16S and 23S rRNA from both *T. elongatus* and *M. ruber*. cDNA libraries were examined using the Agilent 2100 Bioanalyzer to confirm proper size and construction and were sequenced on an Illumina NextSeq 500 sequencer. Reads from all samples were aligned to the genomes of *T. elongatus* BP-1 (NCBI accession no. [NC\\_004113](#)) and the RAST gene model of *Meiothermus ruber* strain A (NCBI accession no. [NZ\\_JXOP01000000](#)) using the Burrows-Wheeler Aligner (BWA) with the default settings (44). Gene counts were determined using HTSeq (45) and were normalized first with DESeq2 (46) followed by normalization to the gene length in kilobases. Additional details on RNA sequencing and transcriptomic data analyses are available in the supplemental material.

**Transcriptomic analyses.** mRNA abundance profiles (given in reads per kilobase per million [RPKM]) for each steady-state condition (measured in biological duplicate) were filtered to remove any gene with an average count of zero in any condition and any gene with an average RPKM of <15. Binary culture expression profiles (genes from both organisms) were grouped via correlation-based K-means clustering (see the supplemental material). Prior to clustering, filtering was employed to mask the bottom 30% of genes with the smallest variance across each respective profile (i.e., flat profiles). Genes were determined to be significantly different in their expression when comparing two conditions if they showed a >2.0-fold change in their expression with an adjusted *P* value of <0.05. Significant enrichment (or functional enrichment) was performed as previously described (43). Briefly, enrichment was defined as the percentage of genes of a given function in the profile depicted (for example, increased expression with increased irradiance under binary conditions) divided by the percentage of genes in that same function in the genome as a whole. Enrichment ratios were then determined to be statistically significant using Fisher’s exact test with any ratio with a *P* value of <0.05 classed as significant.

**ROS-RNS measurements.** Relative abundances of reactive oxygen and nitrogen species (ROS-RNS) were measured using a previously reported method (47). Briefly, we used the cell-permeant fluorescent

dye 5-(6)-chloromethyl-2',7'-dichlorodihydrofluorescein diacetate, acetyl ester (CM-H<sub>2</sub>DCFHDA; Cayman Chemicals, Ann Arbor, MI), for which increased dichlorofluorescein (DCF) fluorescence is a proxy measurement of reactive oxygen/nitrogen species; increased fluorescence is proportional to increased intracellular ROS-RNS. Cell suspensions were collected from a steady-state culture and analyzed in triplicate (3 subfractions of cells collected from each steady state). For each replicate, a 1-ml aliquot was treated with 10 mM CM-H<sub>2</sub>DCFHDA freshly dissolved in 100% Me<sub>2</sub>SO (Sigma-Aldrich, St. Louis, MO) to a final concentration of 10 μM. Concurrently, a 1-ml aliquot of control cells was treated with 1 μl of Me<sub>2</sub>SO. Cells were transferred to opaque black 96-well plates (Nunc A/S, Roskilde, Denmark) and incubated in the dark with intermittent shaking for 30 min at room temperature. Fluorescence was measured at 525 nm after excitation at 488 nm on a SpectraMax Gemini XS spectrofluorometer. The control measurements were subtracted from the CM-H<sub>2</sub>DCFHDA-treated samples to correct for nonspecific fluorescence.

**Accession number(s).** Raw sequencing files are available at the NCBI-GEO repository under accession numbers [GSE94125](https://doi.org/10.1128/mSystems.00181-16) and [GSE93859](https://doi.org/10.1128/mSystems.00181-16).

## SUPPLEMENTAL MATERIAL

Supplemental material for this article may be found at <https://doi.org/10.1128/mSystems.00181-16>.

**TEXT S1**, DOCX file, 0.04 MB.

**FIG S1**, PDF file, 0.1 MB.

**FIG S2**, PDF file, 0.2 MB.

**FIG S3**, PDF file, 0.3 MB.

**FIG S4**, PDF file, 0.2 MB.

**FIG S5**, PDF file, 0.1 MB.

**TABLE S1**, PDF file, 0.2 MB.

**TABLE S2**, PDF file, 0.2 MB.

**DATA SET S1**, XLSX file, 0.8 MB.

**DATA SET S2**, XLSX file, 4.4 MB.

## ACKNOWLEDGMENTS

This research was supported by the U.S. DOE Office of Biological and Environmental Research (BER) Genomic Science Program and is a contribution of the Fundamental Scientific Focus Area. A portion of the RNA sequencing was performed by the Environmental Molecular Sciences Laboratory (user project 49356), a national scientific user facility sponsored by DOE BER and located at PNNL. The corresponding author, H.C.B., is grateful for support given by the Linus Pauling Distinguished Postdoctoral Fellowship, a Laboratory Directed Research program at PNNL. PNNL is operated for the DOE by Battelle Memorial Institute under contract DE-AC05-76RLO 1830.

We acknowledge Leo Kucek, Lye Meng Markillie, Charles Resch, Colin J. Brislawn, Moiz Charania, Christopher Overall, Erika Zink, Tom Metz, and Wayne Curtis for their technical assistance and helpful discussions.

## REFERENCES

- Hooper DU, Chapin FS, Ewel JJ, Hector A, Inchausti P, Lavorel S, Lawton JH, Lodge DM, Loreau M, Naeem S, Schmid B, Setälä H, Symstad AJ, Vandermeer J, Wardle DA. 2005. Effects of biodiversity on ecosystem functioning: a consensus of current knowledge. *Ecol Monogr* 75:3–35. <https://doi.org/10.1890/04-0922>.
- Beliaev AS, Romine MF, Serres M, Bernstein HC, Linggi BE, Markillie LM, Isern NG, Chrisler WB, Kucek LA, Hill EA, Pinchuk GE, Bryant DA, Wiley HS, Fredrickson JK, Konopka A. 2014. Inference of interactions in cyanobacterial-heterotrophic co-cultures via transcriptome sequencing. *ISME J* 8:2243–2255. <https://doi.org/10.1038/ismej.2014.69>.
- Bernstein HC, Paulson SD, Carlson RP. 2012. Synthetic *Escherichia coli* consortia engineered for syntrophy demonstrate enhanced biomass productivity. *J Biotechnol* 157:159–166. <https://doi.org/10.1016/j.jbiotec.2011.10.001>.
- Tai V, Paulsen IT, Phillippy K, Johnson DA, Palenik B. 2009. Whole-genome microarray analyses of *Synechococcus-Vibrio* interactions. *Environ Microbiol* 11:2698–2709. <https://doi.org/10.1111/j.1462-2920.2009.01997.x>.
- Aharonovich D, Sher D. 2016. Transcriptional response of *Prochlorococcus* to co-culture with a marine *Alteromonas*: differences between strains and the involvement of putative infochemicals. *ISME J* 10:2892–2906. <https://doi.org/10.1038/ismej.2016.70>.
- Biller SJ, Coe A, Chisholm SW. 2016. Torn apart and reunited: impact of a heterotroph on the transcriptome of *Prochlorococcus*. *ISME J* 10:2831–2843. <https://doi.org/10.1038/ismej.2016.82>.
- Falkowski PG, Barber RT, Smetacek V. 1998. Biogeochemical controls and feedbacks on ocean primary production. *Science* 281:200–207. <https://doi.org/10.1126/science.281.5374.200>.
- Arai T, Kino K. 2008. A cyanophycin synthetase from *Thermosynechococcus elongatus* BP-1 catalyzes primer-independent cyanophycin synthesis. *Appl Microbiol Biotechnol* 81:69–78. <https://doi.org/10.1007/s00253-008-1623-y>.
- Eberly JO, Ely RL. 2012. Photosynthetic accumulation of carbon storage compounds under CO<sub>2</sub> enrichment by the thermophilic cyanobacterium *Thermosynechococcus elongatus*. *J Ind Microbiol Biotechnol* 39:843–850. <https://doi.org/10.1007/s10295-012-1092-2>.
- Onai K, Morishita M, Itoh S, Okamoto K, Ishiura M. 2004. Circadian rhythms in the thermophilic cyanobacterium *Thermosynechococcus elongatus*: compensation of period length over a wide temperature range. *J Bacteriol* 186:4972–4977. <https://doi.org/10.1128/JB.186.15.4972-4977.2004>.
- Zhang P, Battchikova N, Paakkari V, Katoh H, Iwai M, Ikeuchi M, Pakrasi HB, Ogawa T, Aro EM. 2005. Isolation, subunit composition and interaction

- of the NDH-1 complexes from *Thermosynechococcus elongatus* BP-1. *Biochem J* 390:513–520. <https://doi.org/10.1042/BJ20050390>.
12. Abed RM, Dobretsov S, Sudesh K. 2009. Applications of cyanobacteria in biotechnology. *J Appl Microbiol* 106:1–12. <https://doi.org/10.1111/j.1365-2672.2008.03918.x>.
  13. Henry CS, Bernstein HC, Weisenhorn P, Taylor RC, Lee JY, Zucker J, Song HS. 2016. Microbial community metabolic modeling: a community data-driven network reconstruction. *J Cell Physiol* 231:2339–2345. <https://doi.org/10.1002/jcp.25428>.
  14. Nakamura Y, Kaneko T, Sato S, Ikeuchi M, Katoh H, Sasamoto S, Watanabe A, Iriguchi M, Kawashima K, Kimura T, Kishida Y, Kiyokawa C, Kohara M, Matsumoto M, Matsuno A, Nakazaki N, Shimpo S, Sugimoto M, Takeuchi C, Yamada M, Tabata S. 2002. Complete genome structure of the thermophilic cyanobacterium *Thermosynechococcus elongatus* BP-1. *DNA Res* 9:123–130. <https://doi.org/10.1093/dnares/9.4.123>.
  15. Yamaoka T, Satoh K, Katoh S. 1978. Photosynthetic activities of a thermophilic blue-green-alga. *Plant Cell Physiol* 19:943–954.
  16. Thiel V, Tomsho LP, Burhans R, Gay SE, Schuster SC, Ward DM, Bryant DA. 2015. Draft genome sequence of the *Deinococcus-Thermus* bacterium *Meiothermus ruber* strain A. *Genome Announc* 3:e00202-15. <https://doi.org/10.1128/genomeA.00202-15>.
  17. Thiel V, Wood JM, Olsen MT, Tank M, Klatt CG, Ward DM, Bryant DA. 2016. The dark side of the Mushroom Spring microbial mat: life in the shadow of chlorophototrophs. I. Microbial diversity based on 16S rRNA gene amplicons and metagenomic sequencing. *Front Microbiol* 7:919. <https://doi.org/10.3389/fmicb.2016.00919>.
  18. Loginova LG, Egorova LA, Golovacheva RS, Seregina LM. 1984. *Thermus ruber* sp. nov., nom. rev. *Int J Syst Bacteriol* 34:498–499. <https://doi.org/10.1099/00207713-34-4-498>.
  19. Davies J-M, Nowlin WH, Matthews B, Mazumder A. 2010. Temporal discontinuity of nutrient limitation in plankton communities. *Aquat Sci* 72:393–402. <https://doi.org/10.1007/s00027-010-0143-x>.
  20. Bernstein HC, Carlson RP. 2012. Microbial consortia engineering for cellular factories: in vitro to in silico systems. *Comput Struct Biotechnol J* 3:e201210017. <https://doi.org/10.5936/CSBJ.201210017>.
  21. Ward DM, Bateson MM, Ferris MJ, Kühl M, Wieland A, Koeppel A, Cohan FM. 2006. Cyanobacterial ecotypes in the microbial mat community of Mushroom Spring (Yellowstone National Park, Wyoming) as species-like units linking microbial community composition, structure and function. *Philos Trans R Soc Lond B Biol Sci* 361:1997–2008. <https://doi.org/10.1098/rstb.2006.1919>.
  22. Allewalt JP, Bateson MM, Revsbech NP, Slack K, Ward DM. 2006. Effect of temperature and light on growth of and photosynthesis by *Synechococcus* isolates typical of those predominating in the Octopus Spring microbial mat community of Yellowstone National Park. *Appl Environ Microbiol* 72:544–550. <https://doi.org/10.1128/AEM.72.1.544-550.2006>.
  23. Kühl M, Glud RN, Ploug H, Ramsing NB. 1996. Microenvironmental control of photosynthesis and photosynthesis-coupled respiration in an epilithic cyanobacterial biofilm. *J Phycol* 32:799–812. <https://doi.org/10.1111/j.0022-3646.1996.00799.x>.
  24. Kühl M, Lassen C, Jørgensen BB. 1994. Optical properties of microbial mats: light measurements with fiber-optic microprobes, p 149–166. *In* Stal LJ, Caumette P (ed), *Microbial mats*. Springer, New York, NY.
  25. Nowack S, Olsen MT, Schaible GA, Becraft ED, Shen G, Klapper I, Bryant DA, Ward DM. 2015. The molecular dimension of microbial species: 2. *Synechococcus* strains representative of putative ecotypes inhabiting different depths in the Mushroom Spring microbial mat exhibit different adaptive and acclimative responses to light. *Front Microbiol* 6:626. <https://doi.org/10.3389/fmicb.2015.00626>.
  26. Sakshaug E, Bricaud A, Dandonneau Y, Falkowski PG, Kiefer DA, Legendre L, Morel A, Parslow J, Takahashi M. 1997. Parameters of photosynthesis: definitions, theory and interpretation of results. *J Plankton Res* 19:1637–1670. <https://doi.org/10.1093/plankt/19.11.1637>.
  27. Diaz JM, Hansel CM, Voelker BM, Mendes CM, Andeer PF, Zhang T. 2013. Widespread production of extracellular superoxide by heterotrophic bacteria. *Science* 340:1223–1226. <https://doi.org/10.1126/science.1237331>.
  28. González-Flecha B, Demple B. 1995. Metabolic sources of hydrogen peroxide in aerobically growing *Escherichia coli*. *J Biol Chem* 270:13681–13687. <https://doi.org/10.1074/jbc.270.23.13681>.
  29. Bernstein HC, Kesaano M, Moll K, Smith T, Gerlach R, Carlson RP, Miller CD, Peyton BM, Cooksey KE, Gardner RD, Sims RC. 2014. Direct measurement and characterization of active photosynthesis zones inside waste-water remediation and biofuel producing microalgal biofilms. *Bioresour Technol* 156:206–215. <https://doi.org/10.1016/j.biortech.2014.01.001>.
  30. Bernstein HC, Brislawn C, Renslow RS, Dana K, Morton B, Lindemann SR, Song HS, Atci E, Beyenal H, Fredrickson JK, Jansson JK, Moran JJ. 2017. Trade-offs between microbiome diversity and productivity in a stratified microbial mat. *ISME J* 11:405–414. <https://doi.org/10.1038/ismej.2016.133>.
  31. Falkowski PG, Raven JA. 2013. *Aquatic photosynthesis*. Princeton University Press, Princeton, NJ.
  32. Adamska I. 2001. The Elip family of stress proteins in the thylakoid membranes of pro- and eukaryota, p 487–505. *In* Aro E-M, Andersson B (ed), *Regulation of photosynthesis*. Springer, New York, NY.
  33. He Q, Dolganov N, Björkman O, Grossman AR. 2001. The high light-inducible polypeptides in *Synechocystis* PCC6803 expression and function in high light. *J Biol Chem* 276:306–314. <https://doi.org/10.1074/jbc.M008686200>.
  34. Morris JJ, Johnson ZI, Szul MJ, Keller M, Zinser ER. 2011. Dependence of the cyanobacterium *Prochlorococcus* on hydrogen peroxide scavenging microbes for growth at the ocean's surface. *PLoS One* 6:e16805. <https://doi.org/10.1371/journal.pone.0016805>.
  35. Morris JJ, Kirkegaard R, Szul MJ, Johnson ZI, Zinser ER. 2008. Facilitation of robust growth of *Prochlorococcus* colonies and dilute liquid cultures by “helper” heterotrophic bacteria. *Appl Environ Microbiol* 74:4530–4534. <https://doi.org/10.1128/AEM.02479-07>.
  36. Dietz KJ. 2011. Peroxiredoxins in plants and cyanobacteria. *Antioxid Redox Signal* 15:1129–1159. <https://doi.org/10.1089/ars.2010.3657>.
  37. Raven JA. 2011. The cost of photoinhibition. *Physiol Plant* 142:87–104. <https://doi.org/10.1111/j.1399-3054.2011.01465.x>.
  38. Zhu Y, Graham JE, Ludwig M, Xiong W, Alvey RM, Shen G, Bryant DA. 2010. Roles of xanthophyll carotenoids in protection against photoinhibition and oxidative stress in the cyanobacterium *Synechococcus* sp. strain PCC 7002. *Arch Biochem Biophys* 504:86–99. <https://doi.org/10.1016/j.abb.2010.07.007>.
  39. Scott NL, Xu Y, Shen G, Vuletic DA, Falzone CJ, Li Z, Ludwig M, Pond MP, Preimesberger MR, Bryant DA, Lecomte JT. 2010. Functional and structural characterization of the 2/2 hemoglobin from *Synechococcus* sp. PCC 7002. *Biochemistry* 49:7000–7011. <https://doi.org/10.1021/bi100463d>.
  40. Melnicki MR, Pinchuk GE, Hill EA, Kucek LA, Stolyar SM, Fredrickson JK, Konopka AE, Beliaev AS. 2013. Feedback-controlled led photobioreactor for photophysiological studies of cyanobacteria. *Bioresour Technol* 134:127–133. <https://doi.org/10.1016/j.biortech.2013.01.079>.
  41. Bernstein HC, Konopka A, Melnicki MR, Hill EA, Kucek LA, Zhang S, Shen G, Bryant DA, Beliaev AS. 2014. Effect of mono- and dichromatic light quality on growth rates and photosynthetic performance of *Synechococcus* sp. PCC 7002. *Front Microbiol* 5:488. <https://doi.org/10.3389/fmicb.2014.00488>.
  42. Bernstein HC, Charania MA, McClure RS, Sadler NC, Melnicki MR, Hill EA, Markillie LM, Nicora CD, Wright AT, Romine MF. 2015. Multi-omic dynamics associate oxygenic photosynthesis with nitrogenase-mediated H<sub>2</sub> production in *Cyanothece* sp. ATCC 51142. *Sci Rep* 5:16004. <https://doi.org/10.1038/srep16004>.
  43. Bernstein HC, McClure RS, Hill EA, Markillie LM, Chrisler WB, Romine MF, McDermott JE, Posewitz MC, Bryant DA, Konopka AE, Fredrickson JK, Beliaev AS. 2016. Unlocking the constraints of cyanobacterial productivity: acclimations enabling ultrafast growth. *mBio* 7:e00949-16. <https://doi.org/10.1128/mBio.00949-16>.
  44. Sander J, Nowaczyk M, Buchta J, Dau H, Vass I, Deák Z, Dorogi M, Iwai M, Rögner M. 2010. Functional characterization and quantification of the alternative PsbA copies in *Thermosynechococcus elongatus* and their role in photoprotection. *J Biol Chem* 285:29851–29856. <https://doi.org/10.1074/jbc.M110.127142>.
  45. Anders S, Pyl PT, Huber W. 2015. HTSeq—a Python framework to work with high-throughput sequencing data. *Bioinformatics* 31:166–169. <https://doi.org/10.1093/bioinformatics/btu638>.
  46. Love MI, Huber W, Anders S. 2014. Moderated estimation of fold change and dispersion for RNA-seq data with DESeq2. *Genome Biol* 15:550. <https://doi.org/10.1186/s13059-014-0550-8>.
  47. Baroli I, Gutman BL, Ledford HK, Shin JW, Chin BL, Havaux M, Niyogi KK. 2004. Photo-oxidative stress in a xanthophyll-deficient mutant of *Chlamydomonas*. *J Biol Chem* 279:6337–6344. <https://doi.org/10.1074/jbc.M312919200>.